

Relativistic diffusion process and analysis of transverse momentum distributions observed at RHIC

Naomichi Suzuki

*Department of Comprehensive management, Matsumoto University, Matsumoto, Japan**

Minoru Biyajima

Department of Physics, Shinshu University, Matsumoto, Japan †

Large transverse momentum distributions of identified particles observed at RHIC are analyzed by a relativistic stochastic model in the three dimensional rapidity space. Temperature for inclusive reactions is estimated.

PACS numbers: 25.75.-q, 13.85.Ni, 02.50.Ey

I. INTRODUCTION

At RHIC colliding energy of nuclei becomes up to 200 GeV, and thousands of particles are produced per event. To describe such many particle system, a sort of collective approach will be useful. One-particle rapidity or pseudo-rapidity distributions observed at RHIC are well described by the Ornstein-Uhlenbeck process [1].

As for the transverse momentum p_T distribution observed at RHIC, it has a long tail in the GeV region compared with an exponential distribution in p_T .

In reference [2], an empirical formula for large p_T distributions at polar angle $\theta = \pi/2$,

$$E \frac{d^3\sigma}{d^3p} \Big|_{\theta=\pi/2} = A \exp[-y_T^2/(2L_T)],$$

$$y_T = \frac{1}{2} \ln \frac{E + |\mathbf{p}_T|}{E - |\mathbf{p}_T|}, \quad (1)$$

was proposed from the analogy of Landau's hydrodynamical model. In Eq.(1), E denotes energy of an observed particle, L_T is a parameter, and y_T is called the transverse rapidity. Equation (1) well describes the large p_T distributions for $p + p \rightarrow \pi^0 + X$ and $p + p \rightarrow \pi^\pm + X$. However, it cannot be derived from the hydrodynamical model.

The transverse rapidity is defined in the geodesic cylindrical coordinate system in the three dimensional rapidity space. The Lorentz invariant phase volume element in it is given as

$$\frac{d^3p}{E} = m^2 \sinh \xi \cosh \xi dy d\xi d\phi.$$

In the above equation, y denotes the longitudinal rapidity, and ξ denotes the transverse rapidity;

$$y = \ln \frac{E + p_L}{m_T}, \quad \xi = \ln \frac{m_T + |\mathbf{p}_T|}{m},$$

where E, p_L, \mathbf{p}_T and m denote energy, longitudinal momentum, transverse momentum, and mass of the observed particle, respectively, and $m_T = \sqrt{\mathbf{p}_T^2 + m^2}$. It should be noted that y_T coincides with ξ , only if $\theta = \pi/2$.

We have proposed the relativistic diffusion model, and analyzed large p_T distributions for charged particles in $Au + Au$ collisions [3]. The distribution function of it is gaussian-like in radial rapidity, and resemble with Eq.(1) at $\theta = \pi/2$.

In section 2, the relativistic diffusion model is briefly explained. In section 3, analyses of large p_T distributions for identified particles, π^0, π^-, K^- and \bar{p} observed at RHIC [4, 5, 6] are made. Temperature is also estimated from p_T distributions. Final section is devoted to summary and discussions.

II. DIFFUSION EQUATION IN THE THREE DIMENSIONAL RAPIDITY SPACE

For simplicity, we consider the diffusion equation with radial symmetry in the geodesic polar coordinate system,

$$\frac{\partial f}{\partial t} = \frac{D}{\sinh^2 \rho} \frac{\partial}{\partial \rho} \left(\sinh^2 \rho \frac{\partial f}{\partial \rho} \right). \quad (2)$$

with initial condition

$$f(\rho, t = 0) = \frac{\delta(\rho)}{4\pi \sinh^2 \rho}. \quad (3)$$

In Eq.(2), D is a diffusion constant, and ρ denotes the radial rapidity, which is written with energy E , momentum \mathbf{p} and mass m of observed particle,

$$\rho = \ln \frac{E + |\mathbf{p}|}{m}. \quad (4)$$

Inversely, energy and momentum are written respectively as

$$E = m \cosh \rho, \quad |\mathbf{p}| = \sqrt{p_L^2 + \mathbf{p}_T^2} = m \sinh \rho. \quad (5)$$

The solution [7, 8] of Eq.(2) with the initial condition (3) is given by

$$f(\rho, t) = (4\pi Dt)^{-3/2} e^{-Dt} \frac{\rho}{\sinh \rho} \exp \left[-\frac{\rho^2}{4Dt} \right].$$

*Electronic address: suzuki@matsu.ac.jp

†Electronic address: mbiyajima@azusa.shinshu-u.ac.jp

A physical picture described by Eqs.(2) and (3) is as follows; After a collision of nuclei, particles are produced at the origin of rapidity space expressed by Eq.(3). Then those particles propagate according to the diffusion equation (2). In the course of the space time development, energy is supplied from the leading particle system (collided nuclei) to the produced particle system. Number density of particles becomes lower and at some (critical) density, interactions among secondary particles cease, and particles become free.

We can analyze transverse momentum (rapidity) distributions at fixed polar angle θ , using the equation,

$$f(\rho, t) = C \frac{\rho}{\sinh \rho} \exp \left[-\frac{\rho^2}{2\sigma(t)^2} \right],$$

$$\sigma(t)^2 = 2Dt, \quad (6)$$

with parameters, C and $\sigma(t)^2$, [9]. where transverse momentum is given by $|\mathbf{p}_T| = m \sinh \rho \sin \theta$

III. ANALYSIS OF p_T DISTRIBUTIONS OBSERVED AT RHIC

Transverse momentum (p_T) distributions of identified particles observed by the PHENIX collaboration [4, 5, 6] are analyzed. The results on p_T distribution in $p + p \rightarrow \pi^0 + X$ is shown in Fig. 1. Solid curve shown in Fig.1 is drawn by the use of Eq.(6), parameters of which are estimated with the least mean square method, and are shown in Table 1. The results on p_T distributions in $Au + Au \rightarrow \pi^0 + X$ are shown in Fig. 2 and Table 2. Observed p_T distributions on π^0 both in $p+p$ and $Au+Au$ collisions are well described by Eq.(6).

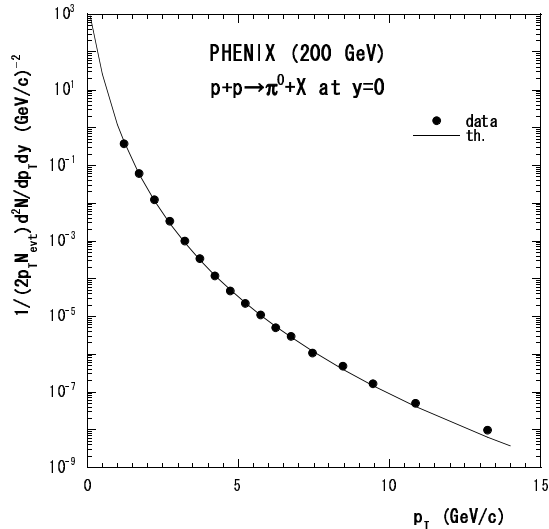


FIG. 1: p_T distribution for $p + p \rightarrow \pi^0 + X$ at $y = 0$ [4]

The results on $Au + Au \rightarrow \pi^- + X$ are shown in Fig. 3 and Table 3. As is seen from Fig.3 and Table 3, fitting

TABLE I: Estimated parameters on p_T distributions in $p + p \rightarrow \pi^0 + X$ at $y = 0$ at $\sqrt{s} = 200$ GeV [4]

C	$\sigma(t)^2$	$\chi^2_{min}/n.d.f.$
1388.0 ± 121.5	0.602 ± 0.004	12.4/15

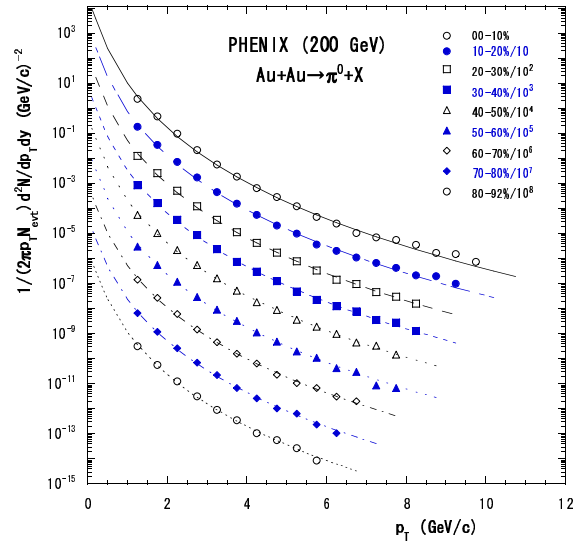


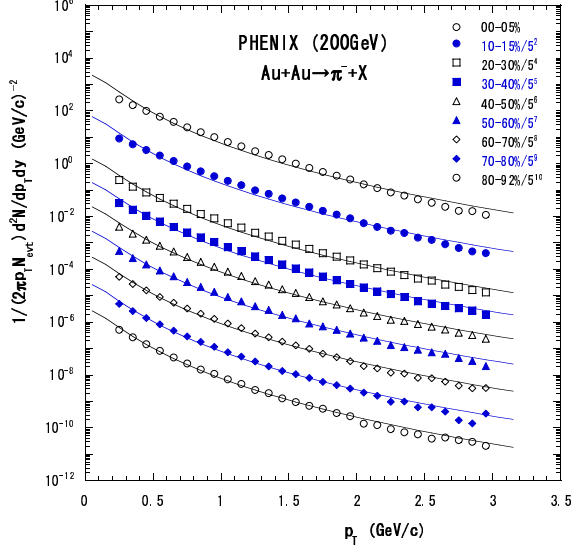
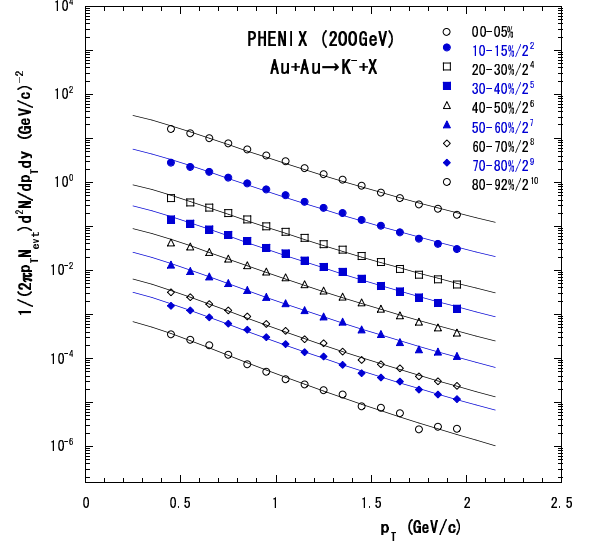
FIG. 2: p_T distribution for $Au + Au \rightarrow \pi^0 + X$ at $y = 0$ [5]

of the theoretical curve to the observed p_T distribution is gradually improved as the centrality cut increases, in other words, the average number of participant nucleons decreases.

The results on $Au + Au \rightarrow K^- + X$ are shown in Fig. 4 and Table 4, and those in $Au + Au \rightarrow \bar{p} + X$ are shown in Fig. 5 and Table 5. As can be seen from Figs.4 and 5, and Tables 4 and 5, fitting of the theoretical curve to the observed p_T distribution are better than those in $Au + Au \rightarrow \pi^- + X$, and become much better as the centrality cut increases.

TABLE II: Estimated parameters on p_T distributions in $Au + Au \rightarrow \pi^0 + X$ at $y = 0$ at $\sqrt{s} = 200$ GeV [5]

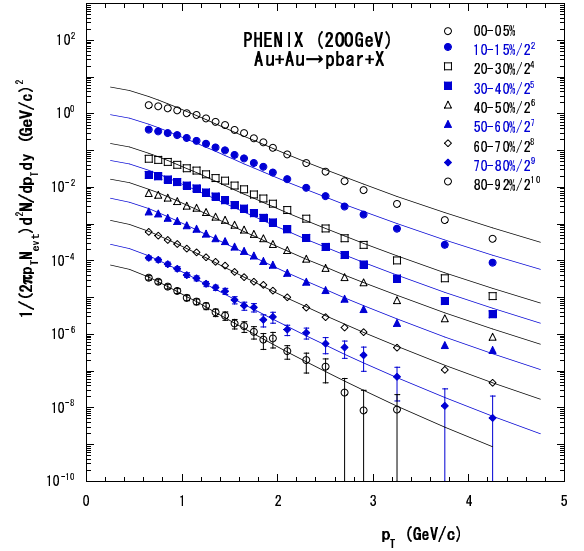
centrality	C	$\sigma(t)^2$	$\chi^2_{min}/n.d.f.$
00-10%	16088 ± 2003	0.574 ± 0.005	27.3/16
10-20%	1161.5 ± 1390.1	0.580 ± 0.005	20.0/15
20-30%	7345.9 ± 922.7	0.586 ± 0.005	14.9/13
30-40%	4378.8 ± 569.3	0.593 ± 0.005	15.7/13
40-50%	2559.8 ± 345.1	0.600 ± 0.006	9.4/12
50-60%	1425.3 ± 194.3	0.599 ± 0.007	12.4/12
60-70%	527.1 ± 78.9	0.617 ± 0.008	8.2/10
70-80%	241.2 ± 39.6	0.616 ± 0.009	7.2/9
80-92%	123.0 ± 24.7	0.611 ± 0.011	5.0/8

FIG. 3: p_T distribution for $Au + Au \rightarrow \pi^- + X$ at $y = 0$ [6]FIG. 4: p_T distribution for $Au + Au \rightarrow K^- + X$ at $y = 0$ [6]TABLE III: Estimated parameters on p_T distributions in $Au + Au \rightarrow \pi^- + X$ at $y = 0$ at $\sqrt{s} = 200$ GeV [6]

centrality	C	$\sigma(t)^2$	$\chi^2_{min}/n.d.f$
00-05%	2539.6 ± 88.8	0.701 ± 0.007	522.8/26
05-10%	2092.7 ± 73.7	0.710 ± 0.008	447.4/26
10-15%	1692.0 ± 59.9	0.718 ± 0.008	390.7/26
15-20%	1391.1 ± 49.9	0.724 ± 0.008	319.4/26
20-30%	1052.8 ± 37.5	0.727 ± 0.008	278.5/26
30-40%	667.0 ± 24.4	0.736 ± 0.009	144.8/26
40-50%	409.8 ± 15.4	0.736 ± 0.009	144.8/26
50-60%	241.2 ± 9.3	0.731 ± 0.010	114.4/26
60-70%	125.4 ± 5.1	0.724 ± 0.010	94.3/26
70-80%	57.4 ± 2.5	0.719 ± 0.012	60.4/26
80-92%	29.5 ± 1.4	0.708 ± 0.013	42.0/26

TABLE IV: Estimated parameters on p_T distributions in $Au + Au \rightarrow K^- + X$ at $y = 0$ at $\sqrt{s} = 200$ GeV [6]

centrality	C	$\sigma(t)^2$	$\chi^2_{min}/n.d.f$
00-05%	44.75 ± 2.81	0.456 ± 0.019	9.45/14
05-10%	37.05 ± 2.33	0.457 ± 0.019	8.67/14
10-15%	30.82 ± 1.93	0.453 ± 0.018	10.77/14
15-20%	25.69 ± 1.62	0.451 ± 0.018	8.52/14
20-30%	19.17 ± 1.21	0.450 ± 0.018	7.07/14
30-40%	12.92 ± 0.82	0.437 ± 0.017	8.37/14
40-50%	7.86 ± 0.50	0.431 ± 0.017	6.57/14
50-60%	4.55 ± 0.31	0.420 ± 0.018	3.85/14
60-70%	2.27 ± 0.16	0.409 ± 0.019	4.44/14
70-80%	1.01 ± 0.08	0.396 ± 0.021	3.60/14
80-92%	0.50 ± 0.04	0.386 ± 0.025	7.44/14

FIG. 5: p_T distribution for $Au + Au \rightarrow \bar{p} + X$ at $y = 0$ [6]

In order to estimate the temperature for inclusive reactions from our analysis, we consider the approximate expression for Eq.(6) in the small $|\mathbf{p}_T|$ region. When $\rho \ll 1$, $\sinh \rho \simeq \rho$. Then, Eq.(6) reduces to

$$f(\rho, t) = C \exp \left[-\frac{\rho^2}{2\sigma(t)^2} \right]. \quad (7)$$

Equation (7) should coincide with the Maxwell distribution,

$$f(\mathbf{v}) = \left(\frac{m}{2\pi kT} \right)^{3/2} \exp \left[-\frac{m\mathbf{v}^2}{2kT} \right].$$

TABLE V: Estimated parameters on p_T distributions in $Au + Au \rightarrow \bar{p} + X$ at $y = 0$ at $\sqrt{s} = 200$ GeV [6]

centrality	C	$\sigma(t)^2$	$\chi^2_{min}/n.d.f$
00-05%	6.48 ± 0.29	0.296 ± 0.008	100.1/20
05-10%	5.49 ± 0.25	0.296 ± 0.008	84.31/20
10-15%	4.57 ± 0.21	0.297 ± 0.008	75.89/20
15-20%	3.85 ± 0.18	0.296 ± 0.008	65.83/20
20-30%	3.04 ± 0.14	0.287 ± 0.008	64.19/20
30-40%	2.10 ± 0.10	0.281 ± 0.008	39.75/20
40-50%	1.30 ± 0.07	0.277 ± 0.009	21.33/20
50-60%	0.79 ± 0.05	0.266 ± 0.010	10.40/20
60-70%	0.40 ± 0.03	0.254 ± 0.012	2.23/20
70-80%	0.18 ± 0.02	0.239 ± 0.016	6.29/20
80-92%	0.10 ± 0.01	0.225 ± 0.019	3.18/20

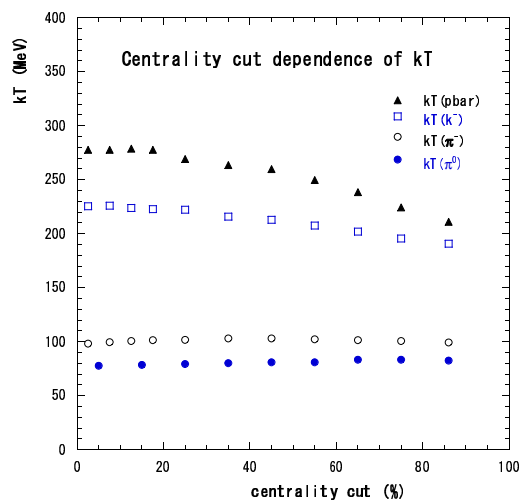


FIG. 6: Centrality cut dependence of temperature kT estimated from p_T distributions in $Au + Au$ collisions

Then we have an identity,

$$kT = m\sigma(t)^2. \quad (8)$$

From Eq.(8), we can estimate the temperature kT of inclusive reactions for observed particle with mass m . The results are shown in Fig. 6. We use $m_{\pi^0} = 135$, $m_{\pi^-} = 140$, $m_{K^-} = 494$, and $m_{\bar{p}} = 938$ MeV.

The estimated temperature kT from the p_T distribution for π^0 is about 80 MeV, and that for π^- is about 100 MeV. These temperatures are almost independent from the centrality cut. On the other hand, the temperature for K^- distributions gradually decreases from 230 MeV to 190 MeV, as the centrality cut increases from 5-10% to 80-92%. That for \bar{p} distributions decreases from 280 MeV to 210 MeV as the centrality cut increases.

Our analysis suggests that K^- and \bar{p} produced at the lowest centrality cut, 0-5%, would keep somewhat earlier memory than π^0 -meson or π^- -meson. It is very interesting to know whether identical particle correlations of K -mesons, protons and so forth depend on the centrality cut or not.

IV. SUMMARY AND DISCUSSIONS

In order to analyze large p_T distributions of charged particles observed at RHIC, a stochastic process in the three dimensional rapidity space is introduced. The solution is gaussian-like in radial rapidity.

Transverse momentum distributions for π^0 and π^- at $y = 0$ at $\sqrt{s} = 200$ GeV observed by the PHENIX collaboration are analyzed. Observed p_T distributions for π^0 in pp and $Au + Au$ collisions are well described by the formula (6), and the result of fitting in $Au + Au$ collisions becomes much better as the centrality cut increases.

The result on transverse momentum distributions for π^- in $Au + Au$ collisions are not good as those for π^0 . However, as the centrality cut increases, the result becomes much improved. This tendency would suggest that the initial condition (3) is simpler for the heavy ion collision process. At the lower centrality cut, collisions among projectile and target particles occur much more times compared with those at higher centrality cut. Therefore, secondary particles produced at each collision may have a certain (collective) velocity distribution wider than the delta function (6) even in the initial stage. In order to include the effect, we should change the initial condition (6), or consider the diffusion equation without radial symmetry in the three dimensional rapidity space.

Acknowledgments

Authors would like to thank RCNP at Osaka university, Faculty of science, Shinshu university, and Matsumoto university for financial support.

[1] M.Biyajima, M.Ide, T.Mizoguchi and N.Suzuki, Prog. Theor. Phys. **108**, 559(2002) ; M.Ide, M. Biyajima and T.Mizoguchi, nucl-th/0302003; see also G.Wolschin, Eur. phys. J. **A5**, 85(1999); Phys. Rev.**C69**, 024906(2004)

[2] Minh Duong-van and P. Carruthers, Phys. Rev. Lett. **31**, 133 (1973)

[3] N.Suzuki and M.Biyajima, Acta Phys. Pol. **B35**, 283(2004)

- [4] S.S.Adler, et al. PHENIX collaboration, Phys. Rev. Lett. **91**, 072301(2003)
- [5] S.S.Adler, et al. PHENIX collaboration, Phys. Rev. Lett. **91**, 241803(2003)
- [6] S.S.Adler, et al. PHENIX collaboration, nucl-ex/0307022
- [7] F.I.Karpelevich, V.N.Tutubalin and M.G.Shur, Theory Prob. Applications, **4**, 432(1959); S.A.Molchanov, Russian Math. Surveys, **30**, 1007(1976)
- [8] N.Suzuki and M.Biyajima, in preparation
- [9] Somewhat different analyses based on statistical models and the different stochastic model have been made in M.Biyajima et al, hep-ph/0403063